1 **Title**

2 Contribution of microorganisms with the Clade II nitrous oxide 3 reductase to suppression of surface emissions of nitrous oxide

4 **Authors**

5 *Kristopher A. Hunt[1*], Alex V. Carr[2,3], Anne E. Otwell[1], Jacob J. Valenzuela[3], Kathleen S.*
6 *Walker[4,5], Emma R. Dixon[4,5], Lauren M. Lui[6], Torben Nielsen[6], Samuel Bowman[7], Frederick von*
7 *Netzer[1], Ji-Won Moon[4], Christopher W. Schadt[4], Miguel Rodriguez Jr.[4], Kenneth Lowe[4],*
8 *Dominique Joyner[4,5], Katherine J. Davis[8], Xiaoqin Wu[10], Romy Chakraborty[10], Matthew W.*
9 *Fields[8,9], Jizhong Zhou[10,11,12], Terry C. Hazen[4,5], Adam P. Arkin[6,13], Scott D. Wankel[7], Nitin*
10 *Baliga[2,3], and David A. Stahl[1]*

11 **Affiliations**

12 [1]: Department of Civil and Environmental Engineering, University of Washington, Seattle, WA
13 98195, United States

14 [2]: Department of Molecular Engineering Sciences, University of Washington, Seattle, WA
15 98105, United States

16 [3]: Institute for Systems Biology, Seattle, WA 98109, United States

17 [4]: Biosciences Division, Oak Ridge National Laboratory, Oak Ridge, TN 37830, United States

18 [5]: Department of Civil and Environmental Engineering, University of Tennessee, Knoxville, TN
19 37996, United States

20 [6]: Environmental Genomics and Systems Biology, Lawrence Berkeley National Laboratory,

21 Berkeley, CA 95064, United States

22 [7]: Department of Marine Chemistry and Geochemistry, Woods Hole Oceanographic Institution,

23 Woods Hole, MA 02540, United States

24 [8]: Center for Biofilm Engineering, Montana State University, Bozeman, MT 59717, United

25 States

26 [9]: Department of Microbiology and Cell Biology, Montana State University, Bozeman, MT

27 59717, United States

28 [10]: Climate and Ecosystem Sciences Division, Lawrence Berkeley National Laboratory,

29 Berkeley, CA 94720, United States

30 [11]: Institute for Environmental Genomics and Department of Botany and Microbiology,

31 University of Oklahoma, Norman, OK 73019, United States

32 [12]: State Key Joint Laboratory of Environment Simulation and Pollution Control, School of

33 Environment, Tsinghua University, Beijing 100084, China

34 [13]: Department of Bioengineering, University of California Berkeley, Berkeley, CA 94720,

35 United States

36

37 **Corresponding Author**
38 Kristopher A Hunt
39 616 NE Northlake Pl., Box 355014
40 Seattle, WA 98105
41 (206) 616-6985

42 hunt0362@uw.edu

43

44 **Abstract**

45 The sources and sinks of nitrous oxide, as control emission to the atmosphere, are generally
46 poorly constrained for most environmental systems. Initial depth-resolved analysis of nitrous
47 oxide flux from observation wells and the proximal surface within a nitrate contaminated aquifer
48 system revealed high subsurface production but little escape from the surface. To better
49 understand the environmental controls of production and emission at this site, we used a
50 combination of isotopic, geochemical, and molecular analyses to show that chemodenitrification
51 and bacterial denitrification are major sources of nitrous oxide in this subsurface where low DO,
52 low pH, and high nitrate are correlated with significant nitrous oxide production. Depth-resolved
53 metagenomes showed that consumption of nitrous oxide in the near surface was correlated with
54 an enrichment of Clade II nitrous oxide reducers, consistent with a growing appreciation of their
55 importance in controlling release of nitrous oxide to the atmosphere. Our work also provides
56 evidence for the reduction of nitrous oxide at a pH of 4, well below the generally accepted limit
57 of pH 5.

58

59 Keywords: (5-8)

60 Nitrous oxide, denitrification, chemodenitrification, *nosZ*, isotopic fractionation, flux, pH

61

62 Synopsis (~30 words)

63 The analytic approach developed to identify sources and sinks of nitrous oxide in a low pH, high
64 nitrate environment should provide guidance to the study of other natural or altered systems
65 emitting this potent greenhouse gas.

66 **Introduction**

67 Increasing nitrous oxide in the atmosphere, an ozone-destructive and potent greenhouse gas with
68 an atmospheric half-life of more than 100 years [1], is associated primarily with its emission from
69 low oxygen aquatic systems, wastewater treatment, and systems impacted by changing land use
70 and agriculture. Produced by both biotic and abiotic processes, the only known sink for nitrous
71 oxide below the stratosphere is the microbial reduction to N_2 by the nitrous oxide reductase
72 (NosZ) enzyme. Although nitrous oxide is a thermodynamically more favorable electron
73 acceptor (E° = 1.77 V) than oxygen (E° = 0.815 V), competition experiments with characterized
74 facultative anaerobes have shown that nitrous oxide reduction is not always the preferred
75 electron acceptor over a wide range of oxygen concentrations [2–4]. This could reflect the
76 stoichiometric differences in energy yield for the alternative substrates since oxygen has a higher
77 energy yield than nitrous oxide on a mole of oxidant basis and may be the more relevant limiting
78 substrate in many environments. Regardless of mechanism, what would appear to be a highly
79 favorable electron acceptor even in the presence of oxygen is lost to the atmosphere from many
80 environments, including soils (0.0006 ± 0.0023 μmol m^{-2} s^{-1} [mean ± standard deviation] [5–10]),
81 marine systems (0.0019 ± 0.0035 μmol m^{-2} s^{-1} [11–16]), and freshwater systems (0.0029 ± 0.0068
82 μmol m^{-2} s^{-1} [17]). Since it is primarily the balance between production and microbial consumption
83 that determines the emission to the atmosphere, improved predictive modeling of nitrous oxide
84 emissions will depend on integrated studies designed to resolve the spatial and temporal
85 distribution of its sources and sinks, and better constrain the biotic and abiotic variables
86 influencing those processes.
87

88 Although terrestrial nitrous oxide consumption is recognized to be solely an enzymatic process,
89 both biotic (denitrification, codenitrification, nitrification, nitrifier-denitrification) and abiotic
90 (chemodenitrification) processes control production. Apart from the need to resolve those
91 alternative sources of production, environmental variables influencing consumption by the
92 activities of organisms expressing the Clade I (a.k.a., typical) or Clade II (a.k.a., atypical) NosZ
93 variant may have a significant impact on emissions of nitrous oxide [18–20]. This is suggested by
94 reports of the differential distribution of these variants in diverse ecosystems, including soils and
95 marine oxygen minimum zones, and a few reports of differences in uptake kinetics and
96 sensitivity to oxygen [21–24]. However, there remains limited understanding of physiological
97 differences and the environmental variables controlling the distribution and activity of the two
98 variants. This information is essential for improved modeling of the flux of this environmentally
99 active gas to the atmosphere, as well as for developing management tools for abatement [22].
100
101 Here we present the use of combined activity, molecular, geochemical, gas flux, and isotopic
102 measurements to resolve the sources and sinks of nitrous oxide in a heavily nitrate contaminated
103 low pH groundwater system on the Oak Ridge National Laboratory (ORNL) Reservation [25]. We
104 used the isotopic composition of nitrogen species to qualitatively demonstrate that both biotic
105 and abiotic processes contributed to significant production of nitrous oxide [26], with biotic
106 production correlated with high numbers of *Rhodanobacter* species [27–29]. In turn, isotopic
107 analyses of nitrous oxide consumption from observation wells, showed active biological
108 reduction at pH values as low as 4, well below values generally thought inhibitory for reduction
109 and only previously observed in a *Rhodanobacter* enriched reactor community [30]. An associated
110 depth-resolved genomic characterization of *nosZ* implicated the Clade II variant in the

111 suppression of surface emissions. Thus, at this site organisms expressing the Clade II NosZ
112 appear to be the major contributor to the consumption of nitrous oxide, functioning to largely
113 suppress surface emissions of this potent greenhouse gas [23,24].
114

115 **Material and Methods**

116 *Field Site*. The observation wells characterized in this study are located at the Field Research
117 Center (FRC) on the Oak Ridge National Laboratory (ORNL) Reservation and hydraulically
118 down-gradient of the capped contaminant source, previously the S3 disposal ponds at the Y12
119 site. Leaching of materials disposed in the ponds from radionuclide processing have contributed
120 to a low pH (3-6.5), high nitrate (> 1 M) groundwater contaminated by organics, radionuclides,
121 and heavy metals [31]. Most contamination is distributed in the deeper saturated and variably
122 saturated zones, with less and more variable contamination in the vadose zone, the region of
123 sediment below the ground surface and above the variably saturated zone [32].
124

125 *Quantification of nitrous oxide flux.* Nitrous oxide and carbon dioxide fluxes from multiple
126 well-heads were quantified using a Picarro gas analyzer (G2508), recirculating pump (A0702),
127 Eosense multiplexer (eosMX), and Eosense flux chambers (eosAC) with 30 m connections
128 between the chambers and multiplexer unit. Flux chambers were mounted on 6 wells located in
129 an area immediately hydraulically down-gradient of the capped S3 disposal ponds (Figure 1).
130 Flux values were determined by averaging the slope of ppm vs time from a 60 second window
131 over data collected from 2 to 5 minutes after purging the connections. The complete analysis
132 and data are available in the supplemental material at 10.6084/m9.figshare.24196218. The limit
133 of flux detection for this system was approximately 10^{-4} and 10^{-2} μmol m^{-2} s^{-1} for nitrous oxide

134 and carbon dioxide, respectively [33]. Flux from each location was normalized to the surface area
135 of the flux chamber for surface measurements or the cross-sectional area of the well casing for
136 well measurements (Table S1).

137

138 *Assays for biotic and abiotic nitrous oxide production activity in the subsurface.* Groundwater
139 biomass collected on filters was used for acetylene block characterization. Approximately 2
140 liters of groundwater was collected on a 0.22 µm PES membrane filter (Sterlitech) by vacuum
141 filtration and used to inoculate 160 mL serum bottles containing 50 mL of filtered groundwater
142 with and without nutrient amendment, and with and without acetylene. Each serum bottle
143 received 1/8 segment of the filter, allowing duplicate incubations. Nitrate and/or organic carbon
144 were amended via 2.5 ml of 100 mM sodium nitrate solution or a solution containing 100 mM
145 sodium lactate, sodium acetate, monosodium glutamate, and sodium benzoate. The final
146 concentration of nitrate and carbon added were 4.5 mM each, but this does not account for any
147 carbon or nitrogen present in the original sample. Acetylene was added to the headspace to a
148 final concentration of 1% from a 10% acetylene stock in dinitrogen and the bottles incubated in
149 the dark at ambient temperature (22 °C). Nitrous oxide accumulation in the headspace was
150 quantified by GC-ECD over a four-day period, collecting gas samples in 12 ml exetainers by 2.5
151 ml syringe transfer on day 0, 1 ml on day 2 and 0.5 ml on day 4.

152

153 *Analysis of nitrate, nitrite, and nitrous oxide isotopic composition.* Environmental samples for
154 nitrogen and oxygen isotopic characterization were collected from eight wells on October 2, 17,
155 30, and November 13, 2019 (Figure 1). Samples for nitrous oxide analysis were collected by
156 pumping approximately 100 g of unfiltered groundwater directly into 1 L mylar sampling bags

157 (Restek 22950) to minimize off-gassing. Each bag contained 0.5 ml of 10 M NaOH, to achieve a
158 pH of at least 12 for sample preservation before shipping to the Woods Hole Oceanographic
159 Institution (WHOI) for analysis. All nitrous oxide sampling materials were flushed with
160 dinitrogen gas (Airgas, Radnor PA) before sample collection to minimize atmospheric
161 contamination. Groundwater for nitrate and nitrite analysis was filtered (0.2 μm PES) and stored
162 in 20 ml Nalgene scintillation vials (ThermoFisher 2003-9050) with minimal headspace before
163 shipping to WHOI for analysis. Water samples for analysis of water δ^2H & $\delta^{18}O$ were filtered
164 through 0.2 μm PES syringe filters and stored without a headspace in 2 ml glass GC vials
165 (ThermoFisher C4010-1W) sealed with septa screw caps (ThermoFisher C4010-40A) before
166 shipping to the University of California at Davis for analysis by Off-Axis Integrated Cavity
167 Output Spectroscopy (Off-Axis ICOS). All samples were stored at 4 °C before shipping.
168

169 Nitrate stable N and O isotope composition was determined using the denitrifier method, wherein
170 nitrate was quantitatively converted to nitrous oxide by a cultured denitrifying bacteria lacking
171 nitrous oxide reductase [34,35]. Approximately 20-40 nmol of sample nitrate was used to produce
172 nitrous oxide, which was purified and cryogenically trapped using a customized purge-and-trap
173 under continuous flow of helium before introduction to an Isoprime100 isotope ratio mass
174 spectrometer (IRMS). Nitrate isotope reference materials (USGS 32, USGS 34 and USGS 35)
175 were analyzed periodically to correct any size or drift and to normalize sample isotope
176 composition. Typical reproducibility for $\delta^{15}N$ was +/- 0.3‰ and for $\delta^{18}O$ is +/- 0.4‰.
177 Concentrations of nitrate (working range of 0.5–800 mg/L) were determined on a Dionex™ ICS-
178 2100 (ThermoFisher Scientific, USA) equipped with an autosampler (Dionex AS40) and an
179 Dionex IonPac™ AS11-HC column (4 x 250 mm) at room temperature with a KOH effluent

180 gradient of 0–60 mM at 1.0 ml/min. The nitrate concentrations at this site were more than 700-
181 fold higher than accompanying nitrite concentrations, therefore the impact of nitrite on the
182 analysis of nitrate would be less than the error of the measurement.
183
184 Nitrite stable N and O isotope composition was determined after conversion to nitrous oxide in
185 acetic-acid buffered sodium azide [36], followed by analysis using the same purge-and-trap system
186 described above. Isotopic ratios are reported in reference to calibrated values of internal lab
187 nitrite standards (WILIS 10, WILIS 11 and WILIS 20). Typical reproducibility for $\delta^{15}N$ and
188 $\delta^{18}O$ is +/- 0.2‰ and +/- 0.3‰, respectively.
189
190 Nitrous oxide isotope analyses were conducted as follows. A 0.2 to 2 ml subsample of the
191 headspace from the multi-layer foil sampling bags was injected into a 25 ml serum bottle
192 previously purged with ultra-high purity helium. Subsamples of this primary dilution were
193 injected into evacuated 20 ml autosampler vials for analysis on the purge-and-trap system.
194 Repeat analyses were conducted to account for large variations in nitrous oxide concentrations of
195 field samples. Isotope ratios ($\delta^{15}N$ and $\delta^{18}O$) were normalized by regular comparison to analyses
196 of USGS 51 and USGS 52, which have similar $\delta^{15}N$ and $\delta^{18}O$ but differing site preference (i.e.,
197 the difference between the position specific $\delta^{15}N$ composition in the central alpha versus outer
198 beta position in the nitrous oxide molecule), using a semi-automated aliquot system on the
199 purge-and-trap. A range of injection volumes of nitrous oxide isotopic analyses from reference
200 tank was used to correct for any injection volumes linearity effects. Typical reproducibility for
201 $\delta^{15}N$ and $\delta^{18}O$ was +/- 0.3‰ and +/- 0.4‰, respectively, and +/- 1.0‰ for site preference.

202 Normalized isotopic signatures were calculated as described in Yu *et. al.* 2020 [26], equations can
203 also be found in the supplemental materials.
204
205 *Depth resolved metagenomic analysis of denitrification gene distribution in sediment cores.*
206 DNA recovered from sediment samples was sequenced using the Illumina platform for
207 metagenome assembly. DNA extraction, sequencing, read quality control, and assembly are
208 described in (Lui et al. 2024) [37]. Briefly, DNA was extracted using the Qiagen PowerMax soil
209 kit with some modifications as described in Lui et al 2024 and Wu et al 2023 and prepped with
210 the Illumina Nextera Flex kit (now called the Illumina DNA Prep kit) [37,38]. Reads were
211 deposited in NCBI's Sequence Read Archive in BioProject PRJNA1001011 under accession
212 numbers SAMN36786281-SAMN36786357. Illumina reads were quality filtered and trimmed
213 using BBTools 38.86 and assembled with SPAdes Version 3.15.4 [39–41].
214
215 A table of metagenome parameters and relevant sample information is included in the
216 supplemental material (Table S3). Samples were co-assembled if they were sample replicates
217 from the same groundwater or sediment sample. Co-assemblies are outlined in Table 1 of Lui et
218 al 2024. Genes were called using Prodigal Version 2.6.3 with parameters "-c -n -p meta" [42].
219 Gene annotation was accomplished using eggNOG-mapper version 2.1.7 with parameters "-m
220 diamond --query_cover 50 --subject_cover 50" [43]. Individual genes (e.g., nosZ) were extracted
221 using textual search on the annotation output. Quality-filtered and trimmed reads were mapped
222 to contigs to obtain coverage values using BWA version 0.7.17-r1188 [44]. We used the BWA-
223 MEM algorithm with the default parameters. Average coverage was calculated for each contig
224 by dividing the total number of bases mapped to the contig by the length of the contig. Relative

225 abundance of a gene was determined by summing the average coverage of each contig that
226 contained that gene and normalizing to the total mapped reads of that sample.

227 **Results**

228 *Impact of groundwater recharge on the chemical and isotopic composition of nitrogen oxides at*
229 *the FRC.* The sampling of FRC groundwater from the saturated zone bracketed a dry period
230 (August 29th, 2019 - October 16th, 2019) followed by a two-week period of frequent rains that
231 raised the water table (Figure 2 and S2). The rain-associated recharge was correlated with an
232 approximate 0.5 unit drop in pH for all wells except for FW106, which remained at pH 4. The
233 dissolved oxygen was relatively constant at 0.2 +/- 0.2 mg/l for most wells. Relatively invariant
234 isotopic composition of the water ($\delta^{18}O$ and $\delta^{2}H$) during the observation period suggested that
235 rain increased groundwater flow at the observed depths but did not alter its sources (Figure S3).
236 However, isotopic composition did show that some nearby deep wells received water from at
237 least two different sources, pointing to significant hydraulic heterogeneity that was also reflected
238 in changing nitrate concentrations over time. Groundwater nitrate originating from the former
239 S3 waste disposal pond generally was within the range of 10 to 100 mM but reached 140 mM in
240 some wells in the later part of the sampling period (October 30th, 2019).
241

242 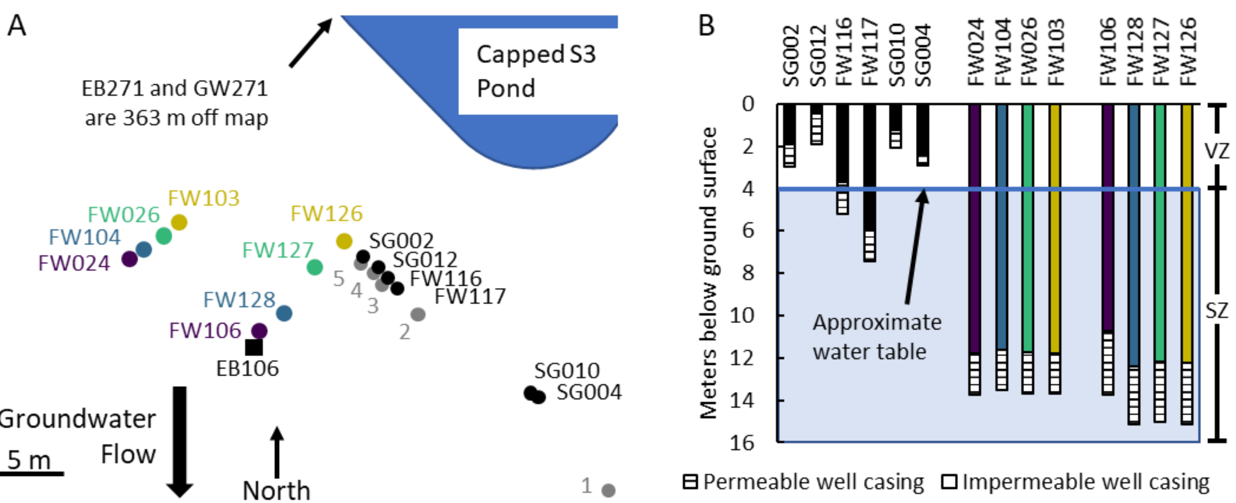

243 **Figure 1.** A) Schematic of the field site showing the location of the contamination source
244 (capped S3 pond) and sampling locations. Wells sampled for isotopic analysis and chemistry are
245 represented by colored circles. Wells monitored for nitrous oxide flux are shown as black
246 circles. Surface positions for flux measurements are marked with grey circles. The location of
247 the sediment core EB106 is marked with a black square. B) Profile of well screen depths (striped
248 region) used for ground water sampling. The approximate location of the ground water table is
249 designated with a horizontal blue line and the vadose zone (VZ) and saturated zone (SZ) are
250 annotated to the right of the figure.
251

252

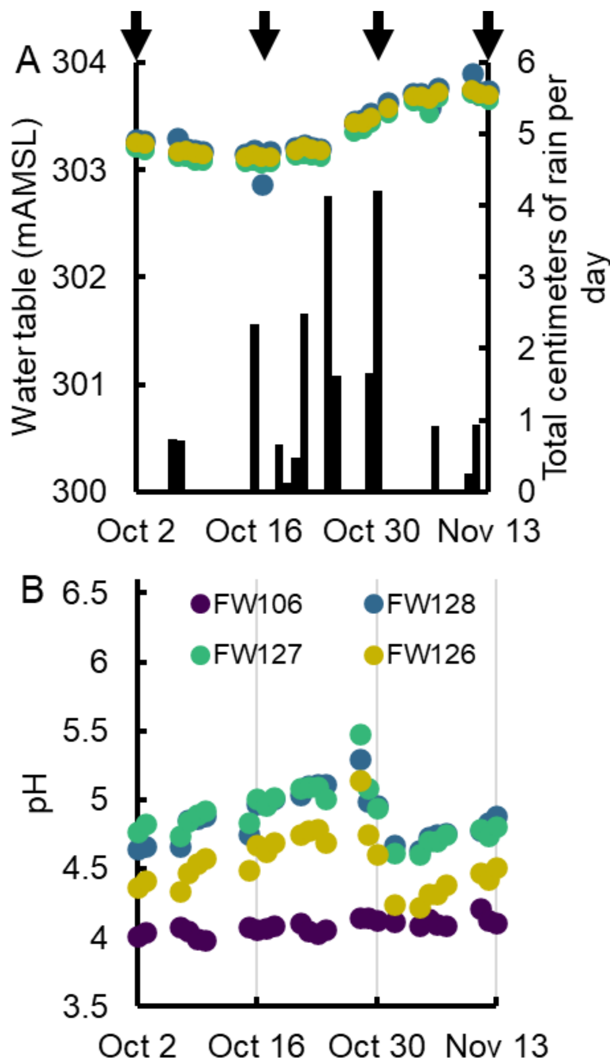

253 **Figure 2.** Impact of rain events on water table height (A) and pH (B) of selected wells. The

254 months prior to sampling for isotopes (arrows, A) received less than 0.5 cm of rain per day. That

255 dry period was followed by days of significant rain (bar plot, A) that restored the water table

256 (colored filled circles, A) and coincided with a drop in pH (colored filled circles, B) for all but

257 one well (FW106, purple).

258

259 The isotopic composition of groundwater nitrate from the sampling wells was relatively constant

260 but enriched in ^{15}N and ^{18}O relative to commonly reported values for synthetic nitrate (Figure

261 S4), the expected source of nitrate in the S3 ponds. The relatively constant isotopic composition
262 of nitrate throughout the observation period, despite excursions in concentration, suggested a
263 combination of 1) an isotopically enriched source nitrate and 2) variable dilution and reduction
264 of the primary source near the disposal pond before entering the groundwater or in transit to the
265 sampled well (Figures 3 and S5). A notable exception was observed in groundwater from
266 FW106, where the nitrate contributing to increased well-water concentration following the rain
267 event exhibited markedly lower $\delta^{15}N$ and $\delta^{18}O$ values. Thus, there appear to be multiple sources
268 of nitrate, some having experienced less denitrification and therefore maintaining proportionately
269 lower $\delta^{15}N$ and $\delta^{18}O$ values.
270
271 The time dependent nitrate concentrations and isotopic composition of groundwater in FW106
272 could also reflect the importance of reactive transport in the system. An increase in the
273 subsurface flow rate following rain (Figure 2A) likely reduced the period of time the nitrate was
274 acted upon by microbial activity, retaining the lighter isotopic signature of the source. The
275 isotopic shifts likely reflect primarily denitrification activity since more than 5 mM ammonia
276 would be required for a measurable impact by nitrification or nitrifier-denitrification, a
277 concentration greatly exceeding reported groundwater values of less than 0.5 mM (Figure S4) [32].
278 Together, these observations reflect the complex hydrology contributing to different local nitrate
279 sourcing in this highly altered system and highlight the need for improved reactive transport
280 modeling of the site.

281

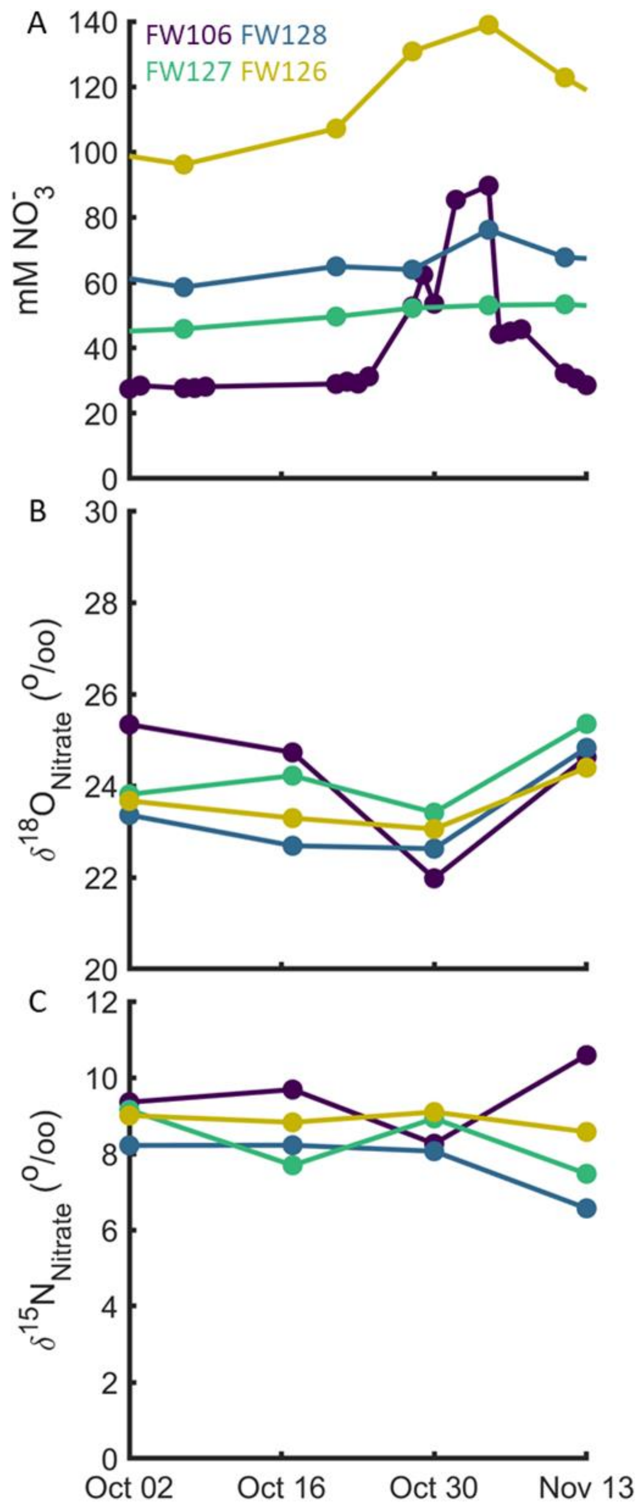

282 **Figure 3.** Nitrate concentration and isotopic composition were relatively constant throughout

283 the time of sampling, indicating limited excursions in reaction or transport, except for FW106.

284 An increase in the nitrate concentration of water sampled from FW106 following rain (A)
285 correlated with a shift to a lighter isotopic composition (B and C), suggesting a more variable
286 influence of nitrate reduction on this water mass.
287
288 *Sources and sinks of subsurface nitrous oxide*. Nitrous oxide was quantified both in groundwater
289 and as mass fluxes from separate wells screened at distinct depths. Here we examine biotic and
290 abiotic sources of production in groundwater through isotopic composition and activity
291 measurements. We consider the gas flux data in relationship to possible nitrous oxide sinks in a
292 following section.
293
294 Multiple processes, both biotic and abiotic, are known to contribute to nitrous oxide production.
295 The primary contributing activities are denitrification by bacteria, archaea, and fungi,
296 nitrification by bacteria and archaea, chemodenitrification, and dissimilatory nitrate reduction to
297 ammonium (DNRA) by bacteria. The individual contributions to nitrous oxide production in an
298 environmental system can be partially resolved by analyzing the natural isotopic composition of
299 nitrous oxide. Analysis of the nitrous oxide site preference (SP) from multiple wells over a
300 several weeks period (Figure 4 and S7) revealed both relatively stable (e.g., FW106, FW127,
301 FW126, and FW103) and highly variable SP patterns (e.g., FW128, FW024, FW026, and
302 FW104), with evidence for major contributions from both denitrification and
303 chemodenitrification based on published meta-analyses of both pure culture and natural systems
304 with defined or verified activity [26].

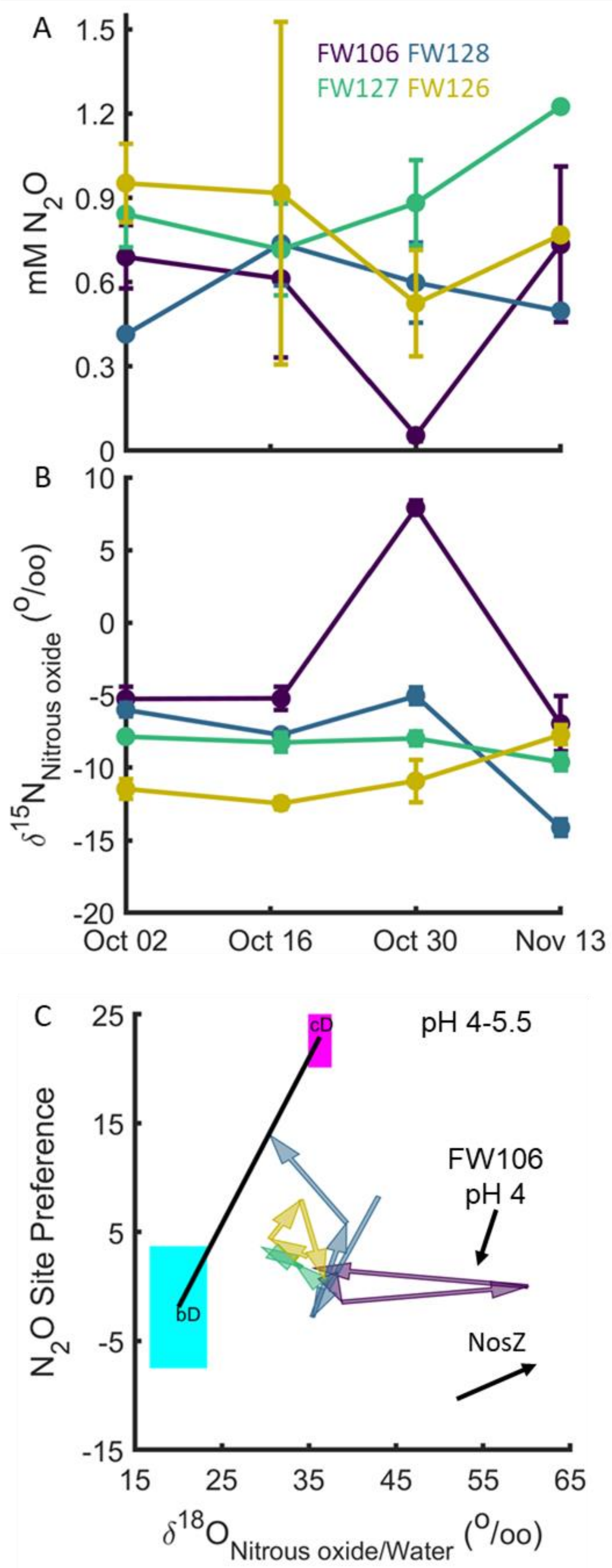

305

306 **Figure 4.** Temporal dynamics of nitrous oxide concentration (A) and isotopic composition (B)
307 in the groundwater. Error bars show standard deviations of at most triplicate technical replicates.
308 Active but variable biotic consumption of nitrous oxide is inferred from the increases in $\delta^{15}N$ (B)
309 and $\delta^{18}O$ (C) associated with its reduction. Among wells and sampling periods, the most active
310 reduction of source nitrous oxide was observed in well FW106 on Oct 30, as reflected by both
311 the depletion of nitrous oxide and its corresponding enrichment in the heavier isotopes (B, C).
312 The site preference (SP) of nitrous oxide and enrichment $\delta^{18}O$ values normalized by the $^{18}O/^{16}O$
313 of the accompanying groundwater (C) are consistent with both a mixed biotic-abiotic source of
314 nitrous oxide and consumption through biotic reduction. Colored arrows denote the time course
315 of compositional change of samples taken from each well as colored in panels A and B. The
316 black arrow indicates the temporal direction in SP and $\delta^{18}O$ composition when only biotic
317 reduction acts on a sample. The solid black line connecting bacterial denitrification (bD, cyan
318 box) and chemodenitrification (cD, magenta box) shows the expected variation in SP for a linear
319 combination of both processes [26]. See supplementary information Figure S7 for additional data.
320
321 The importance of chemodenitrification at this site is also supported by incubations with
322 acetylene to block NosZ activity. Active biological production and consumption of nitrous oxide
323 was observed in groundwater sampled from GW271 in an area of low contamination, up gradient
324 from the primary source of contamination, as shown by nitrous oxide accumulation only when
325 acetylene was added to samples amended with organic carbon and nitrate. Addition of acetylene,
326 organic carbon, and nitrate resulted in accumulation of significant nitrous oxide not observed
327 with acetylene addition alone, indicative of the stimulation of a biotic source of nitrous oxide in
328 areas of low carbon availability (Figure 5). In contrast, nitrous oxide production was observed

329 for all treatments of highly contaminated groundwater sampled from FW106. The stimulation of
330 production by addition of both carbon and acetylene is consistent with nitrous oxide primarily
331 originating from an abiotic source and lesser from a biotic source. Nitrite was present at
332 concentrations ranging from below detection (i.e., <0.5 μM) to 66 μM (mean = 7.8, median =
333 6.2) (Figure S6), consistent with it serving as a short-lived co-reactant in chemodenitrification
334 via iron oxidation as has been reported previously [27]. Although reduced iron or other natural
335 reductants driving abiotic production have not been identified, the total iron concentration in
336 groundwater is in the range of 60 to 180 g per kg of sediment and microbial reduction could
337 provide a source of reduced iron [32].

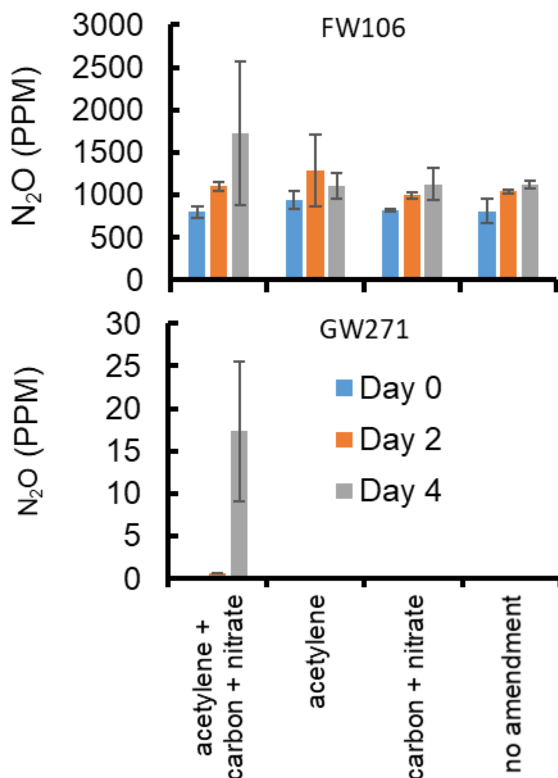

338

339 **Figure 5**. Acetylene block characterization of alternative nitrous oxide sources in FRC
340 groundwater. A significant abiotic source of nitrous oxide in groundwater was supported by
341 addition of acetylene to block NosZ activity. Addition of acetylene to contaminated low pH

342 groundwater sampled from FW106, with and without organic carbon supplementation, showed
343 only a slight increase in production relative to unamended samples (upper panel). In contrast, all
344 production in groundwater from a well (GW271) outside the contamination plume could be
345 attributed to a biotic source when amended with organic carbon, nitrate, and acetylene (lower
346 panel). Error bars represent the standard deviation of duplicate mesocosm experiments taken in
347 November 2016 (FW106) and March 2017 (GW271).

348

349 Biological consumption of nitrous oxide was suggested by elevated $\delta^{18}O$ and $\delta^{15}N$ values of the
350 nitrous oxide pool. Assuming the source was a combination of chemodenitrification and
351 bacterial denitrification, as indicated by a mixing line between their previously reported values,
352 enrichment in $\delta^{18}O$ and $\delta^{15}N$ of the nitrous oxide pool is likely due to a change in the source or
353 an increase in contribution of nitrous oxide reduction (Figure 4 and S7) [26]. The contribution of
354 nitrous oxide reduction to isotopic enrichment was evident in several wells, as exemplified by
355 well FW106. The decrease in nitrous oxide concentration in groundwater received by this well
356 on October 30, 2019 was correlated with strong increases in $\delta^{18}O$ and $\delta^{15}N$ values. The transient
357 increase in nitrous oxide reduction activity appeared to be a system-level response to rainfall
358 associated changes in pH and nitrate concentration (Figure 2, 3, S2, and S5), and presumably
359 other nutrients flushed with this recharge event. However, the high variability in chemistry and
360 biological response among wells co-localized by position and depth is additional evidence for
361 subsurface hydraulic heterogeneity (Figure 4 and S7).

362

363 *Surface and subsurface flux of nitrous oxide*. Nitrous oxide flux was measured at the surface and
364 from wells screened at different depths to identify regions of production and consumption

365 (Figure 6). To correct for diffusion effects through the soil and sediment, the fluxes from wells
366 were multiplied by the relative diffusion coefficient of a gas in homogeneous low porosity sand
367 or clay (porosity = 0.2) compared to open air (D_{soil}/D_{air} = 0.03) (Figures 6 and S9, supplemental
368 material) [45]. This diffusion model is supported by the flux response to rain events (Figure 6)
369 where the increased sediment water content from rain restricted gas flow and increased well
370 concentrations of nitrous oxide. The corrected fluxes were generally the highest near the
371 variably saturated zone and decreased with proximity to the surface. Surface emissions were
372 near the limit of detection and only somewhat higher near FW126, a location known to have
373 higher permeability due to a gravel drainage channel (Supplemental material and Figure S9).
374 The exception to this trend were higher fluxes measured from one shallow well (SG010). The
375 proximity of SG010 to SG004, a well of much lower flux, suggests the higher flux in SG010
376 reflects either channeling due to subsurface heterogeneity or its localization in a hot spot of
377 activity.
378
379 The general shape of the nitrous oxide flux profile suggests that nitrous oxide produced within
380 the saturated and variably saturated zones is consumed by microbiota higher in the sediment
381 column (vadose zone) before reaching the surface. In contrast, carbon dioxide flux, a more
382 general measure of total heterotrophic microbial activity, increased from deeper depths to the
383 near surface before decreasing at the surface. The lower surface flux likely reflects a
384 normalization of flux as noted by the high temporal variability of well measurements (Figure S8)
385 but steady emission from the surface, although autotrophic activity and carbon equilibration may
386 be contributing factors (Figure 6) [46,47]. These profiles both support a metabolically active vadose
387 zone, potentially dominated by heterotrophic activity producing carbon dioxide and respiring

388 available electron acceptors, including nitrous oxide. However, an unusual feature of subsurface
389 fluxes was high variability over a 24-hour period, with the highest fluxes generally observed
390 during the day (Figure S8). Published observations of similar diel variation in surface emissions
391 from a variety of soil systems have been associated with diel variation in temperature [48,49]. Our
392 observations of a diel cycling trend for nitrous oxide in an environment of near-constant
393 temperature suggests a contribution of other factors and the sensitivity of this system to relatively
394 minor shifts in water and nutrient movement, possibly related to surrounding land use.
395

396

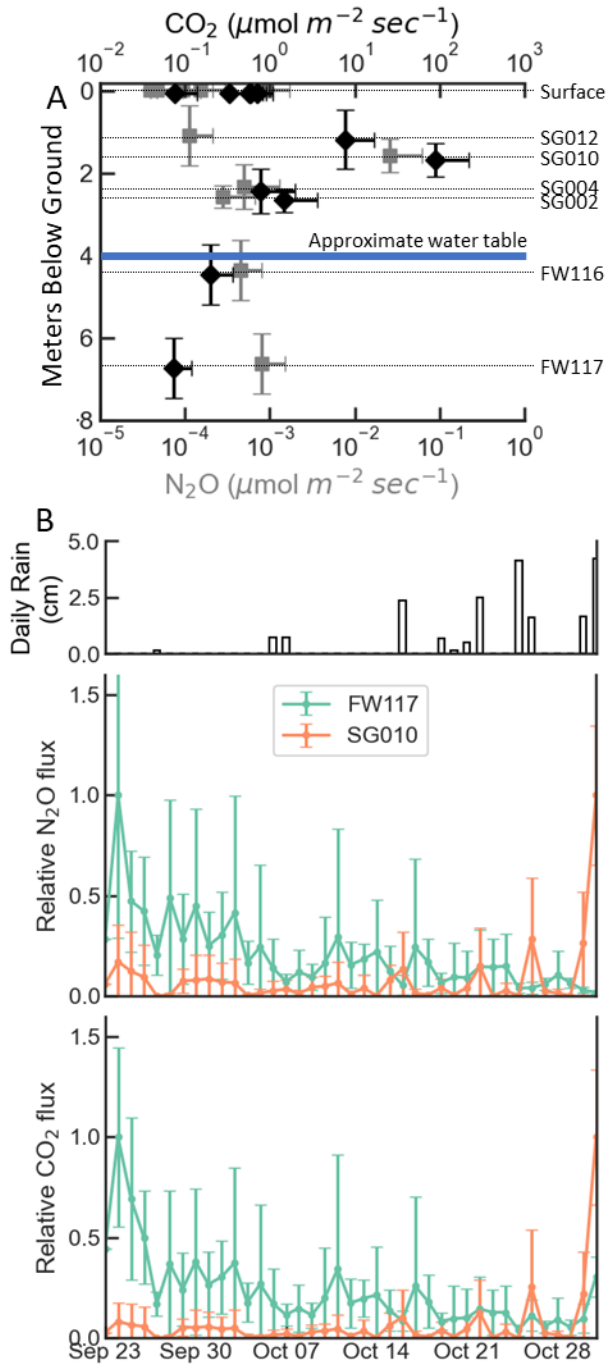

397 **Figure 6.** Nitrous oxide and carbon dioxide subsurface and surface flux. Nitrous oxide and

398 carbon dioxide fluxes were determined from wells screened at different depths to estimate the

399 flux of gas through the sediment column from Sept 22-27, 2019, representing at least 11

400 measurements for each location (A). Relative flux, as plotted, is the flux of a well normalized to

401 the maximum observed for that well. All surface measurements are plotted to highlight their
402 collectively negligible contributions. Two wells, FW117 and SG010, were monitored for an
403 extended time to correlate well measurements with surface measurements taken October 7-9,
404 2019. The deeper well, FW117, was insensitive to rain events while the shallower well, SG010,
405 showed an increased flux on days with rain (B, C). Only FW117 and SG010 were monitored
406 during the rain events.
407
408 *Depth resolved mapping of the genetic potential for nitrous oxide production and consumption.*
409 A metagenomic analysis of soil cores collected from within and outside the contaminant plume
410 was used to examine the depth-resolved relationship between the two *nosZ* variants and nitrous
411 oxide flux. The reductases were identified using co-occurrence of an ancillary gene (*nosR*).
412 NosR is an FMN-binding flavoprotein present only in characterized Clade I organisms and
413 implicated in electron transfer from the quinone pool to NosZ [21]. Since *nosR* is absent in Clade
414 II organisms, the variants can be distinguished by the distribution of *nosZ* and *nosR*. Abundance
415 of Clade I or II encoding populations was determined by multiplying the abundance of *nosR*
416 (Clade I) or *nosZ-nosR* (Clade II) relative to all genes in a sample, respectively, by the cells/gram
417 of sediment at that location as measured previously [32]. This revealed a clear separation by depth
418 in the core (EB106) collected from an area of high subsurface flux and low surface emissions
419 (Figure 7). Clade II was the most abundant variant in the upper vadose zone, both numerically
420 and as a fraction of all *nosZ*, whereas Clade I comprised a higher fraction of the two variants in
421 the more acidic (pH ~4) saturated region immediately above the water table. Thus, organisms
422 expressing Clade II NosZ appear to be a major contributor to the consumption of nitrous oxide in
423 this region of high subsurface nitrous oxide flux, functioning to largely suppress surface

424 emissions of a potent greenhouse gas. This role of Clade II NosZ has also been proposed by
425 others, based on observations in soil and the marine oxygen minimal zones [23,24]. In contrast to
426 the core from within the contaminated zone, nitrous oxide off-gassing from all depths of the core
427 (EB271) collected outside the contaminant plume was orders of magnitude lower than from
428 EB106 immediately following coring [32]. Here vertical stratification of Clade I and Clade II was
429 less apparent, with the two variants more equally distributed with depth.
430

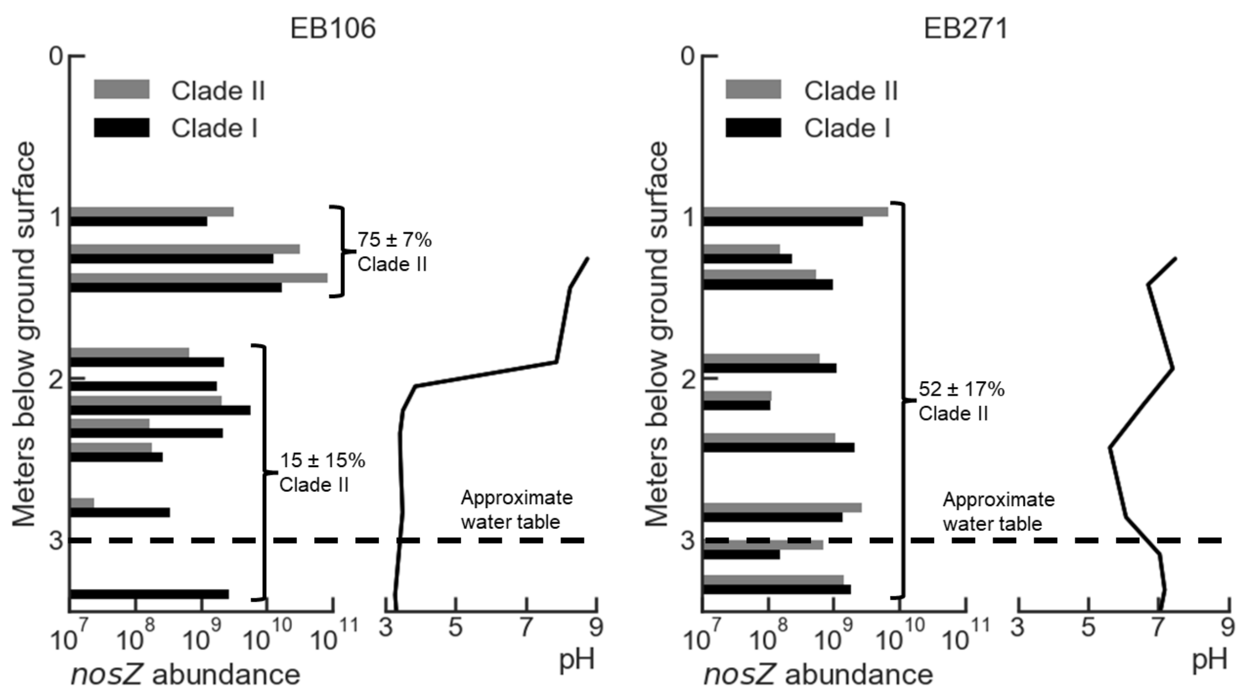

431

432 **Figure 7.** Depth distribution of *nosZ* variants within (EB106) and outside (EB271) the
433 contaminant plume. The water table was approximately 3 meters below the ground surface at the
434 time of sampling.
435

436 Although our analysis clearly implicates Clade II in suppression of nitrous oxide emissions, the
437 physiological and environmental factors controlling the distribution and activity of organisms

438 expressing either variant are very poorly constrained. Some available data points to a higher
439 affinity for nitrous oxide and less inhibition by oxygen [4,19,50]. However, our data point to much
440 more complex environmental controls of distribution and activity. Also, since most of the Clade
441 II containing organisms identified in our metagenomic survey are not represented in any of the
442 major culture collections, a future emphasis on cultivation and isolation of environmentally
443 relevant representatives will be key to constraining models to accurately predict net emission of
444 nitrous oxide from the soil to the atmosphere.
445
446 Another physiologically and environmentally relevant feature of the denitrification pathway,
447 based on complete genome sequence surveys, is the spotty organismal composition of genes in
448 the canonical pathway. Complete pathway organisms appear to be relatively rare, most often the
449 pathway is interrupted or truncated. Some populations encode *nosZ* but lack other denitrification
450 genes, known as nondenitrifying nitrous oxide reducers [51]. One consequence of fragmented
451 pathway distribution is the organismal production of environmentally important intermediates
452 (nitrite, nitric oxide, nitrous oxide), suggesting their importance to combined biotic and abiotic
453 activities, and organismal partnering for achieving complete denitrification. The ecological
454 significance of organismal partnering and environmental conditions conducive to partnering are
455 mostly unrecognized and understudied areas of research.
456
457 The well-grounded dogma that "the environment selects" makes the Oak Ridge Field Research
458 Center an important test bed for refining understanding of the impact of gene variants, organism
459 pathway composition and partnering, and environmental factors governing both biotic and
460 abiotic nitrogen transformation and loss. The environment is not only selective (genotype), but

461 also governs functional activity (phenotype). For example, even among organisms encoding the
462 complete pathway, environmental factors such as pH, metals availability, and oxygen
463 concentration influence the oxidation state of the final nitrogen product. Low pH, as is common
464 at this field site, is well recognized to promote nitrous oxide production by inhibiting NosZ
465 activity [52]. Yet the isotopic composition of nitrous oxide at the ORNL reservation clearly
466 indicates NosZ activity at a pH of 4 (Figure 4). As a more complete collection of field relevant
467 organisms is brought into culture for genetic and physiological characterization, those data will
468 further inform field-based process observations. In turn, ongoing process-directed metagenomic,
469 isotopic, chemical, and activity surveys will serve to identify locations within this contaminated
470 field site for the hypothesis testing essential to developing more predictive models of reactive
471 nitrogen transformation and flux.
472
473 Supporting Information
474 Additional data and figures about instrumentation, well characteristics, metagenome statistics,
475 normalizations, and dynamics of other wells in the area are provided (PDF)
476
477 Acknowledgements
478 This material by ENIGMA – Ecosystems and Networks Integrated with Genes and Molecular
479 Assemblies (http://enigma.lbl.gov), a Science Focus Area Program at Lawrence Berkeley
480 National Laboratory is based upon work supported by the U.S. Department of Energy, Office of
481 Science, Office of Biological & Environmental Research under contract number DE-AC02-
482 05CH11231.

483 References

484 (1) Prather, M. J.; Hsu, J.; DeLuca, N. M.; Jackman, C. H.; Oman, L. D.; Douglass, A. R.;
485 Fleming, E. L.; Strahan, S. E.; Steenrod, S. D.; Søvde, O. A.; Isaksen, I. S. A.; Froidevaux,
486 L.; Funke, B. Measuring and Modeling the Lifetime of Nitrous Oxide Including Its
487 Variability. *Journal of Geophysical Research: Atmospheres* **2015**, *120* (11), 5693–5705.
488 https://doi.org/10.1002/2015JD023267.

489 (2) Qi, C.; Zhou, Y.; Suenaga, T.; Oba, K.; Lu, J.; Wang, G.; Zhang, L.; Yoon, S.; Terada, A.
490 Organic Carbon Determines Nitrous Oxide Consumption Activity of Clade I and II NosZ
491 Bacteria: Genomic and Biokinetic Insights. *Water Res* **2022**, *209*, 117910.
492 https://doi.org/10.1016/j.watres.2021.117910.

493 (3) Suenaga, T.; Riya, S.; Hosomi, M.; Terada, A. Biokinetic Characterization and Activities
494 of N_2O-Reducing Bacteria in Response to Various Oxygen Levels. *Front Microbiol* **2018**,
495 *9*. https://doi.org/10.3389/fmicb.2018.00697.

496 (4) Wang, Z.; Vishwanathan, N.; Kowaliczko, S.; Ishii, S. Clarifying Microbial Nitrous Oxide
497 Reduction under Aerobic Conditions: Tolerant, Intolerant, and Sensitive. *Microbiol Spectr*
498 **2023**. https://doi.org/10.1128/spectrum.04709-22.

499 (5) Braun, R. C.; Bremer, D. J. Nitrous Oxide Emissions in Turfgrass Systems: A Review.
500 *Agron J* **2018**, *110* (6), 2222–2232. https://doi.org/10.2134/agronj2018.02.0133.

501 (6) Panday, D.; Nkongolo, N. V. Soil Water Potential Control of the Relationship between
502 Moisture and Greenhouse Gas Fluxes in Corn-Soybean Field. *Climate* **2015**, *3* (3), 689–
503 696. https://doi.org/10.3390/cli3030689.

504 (7) Castaldi, S.; Bertolini, T.; Valente, A.; Chiti, T.; Valentini, R. Nitrous Oxide Emissions
505 from Soil of an African Rain Forest in Ghana. *Biogeosciences* **2013**, *10* (6), 4179–4187.
506 https://doi.org/10.5194/bg-10-4179-2013.

507 (8) Dobbie, K. E.; Smith, K. A. Impact of Different Forms of N Fertilizer on N_2O Emissions
508 from Intensive Grassland. *Nutr Cycl Agroecosyst* **2003**, *67* (1), 37–46.
509 https://doi.org/10.1023/A:1025119512447.

510 (9) Aliyu, G.; Sanz-Cobena, A.; Müller, C.; Zaman, M.; Luo, J.; Liu, D.; Yuan, J.; Chen, Z.;
511 Niu, Y.; Arowolo, A.; Ding, W. A Meta-Analysis of Soil Background N_2O Emissions from
512 Croplands in China Shows Variation among Climatic Zones. *Agric Ecosyst Environ* **2018**,
513 *267*, 63–73. https://doi.org/10.1016/j.agee.2018.08.003.

514 (10) Sosulski, T.; Szara, E.; Szymańska, M.; Stępień, W.; Rutkowska, B.; Szulc, W. Soil N_2O
515 Emissions under Conventional Tillage Conditions and from Forest Soil. *Soil Tillage Res*
516 **2019**, *190*, 86–91. https://doi.org/10.1016/j.still.2019.03.002.

517 (11) Prosser, J. I.; Hink, L.; Gubry-Rangin, C.; Nicol, G. W. Nitrous Oxide Production by
518 Ammonia Oxidizers: Physiological Diversity, Niche Differentiation and Potential

519 Mitigation Strategies. *Glob Chang Biol* **2020**, *26* (1), 103–118.
520 https://doi.org/10.1111/gcb.14877.

521 (12) Dore, J. E.; Popp, B. N.; Karl, D. M.; Sansone, F. J. A Large Source of Atmospheric Nitrous
522 Oxide from Subtropical North Pacific Surface Waters. *Nature* **1998**, *396* (6706), 63–66.
523 https://doi.org/10.1038/23921.

524 (13) Arévalo-Martínez, D. L.; Kock, A.; Löscher, C. R.; Schmitz, R. A.; Bange, H. W. Massive
525 Nitrous Oxide Emissions from the Tropical South Pacific Ocean. *Nat Geosci* **2015**, *8* (7),
526 530–533. https://doi.org/10.1038/ngeo2469.

527 (14) Trimmer, M.; Chronopoulou, P. M.; Maanoja, S. T.; Upstill-Goddard, R. C.; Kitidis, V.;
528 Purdy, K. J. Nitrous Oxide as a Function of Oxygen and Archaeal Gene Abundance in the
529 North Pacific. *Nat Commun* **2016**, *7*, 1–10. https://doi.org/10.1038/ncomms13451.

530 (15) Muñoz-Hincapié, M.; Morell, J. M.; Corredor, J. E. Increase of Nitrous Oxide Flux to the
531 Atmosphere upon Nitrogen Addition to Red Mangroves Sediments. *Mar Pollut Bull* **2002**,
532 *44* (10), 992–996. https://doi.org/10.1016/S0025-326X(02)00132-7.

533 (16) Quick, A. M.; Reeder, W. J.; Farrell, T. B.; Tonina, D.; Feris, K. P.; Benner, S. G. Nitrous
534 Oxide from Streams and Rivers: A Review of Primary Biogeochemical Pathways and
535 Environmental Variables. *Earth Sci Rev* **2019**, *191* (February), 224–262.
536 https://doi.org/10.1016/j.earscirev.2019.02.021.

537 (17) Hasegawa, K.; Hanaki, K.; Matsuo, T.; Hidaka, S. Nitrous Oxide from the Agricultural
538 Water System Contaminated with High Nitrogen. *Chemosphere - Global Change Science*
539 **2000**, *2* (3–4), 335–345. https://doi.org/10.1016/S1465-9972(00)00009-X.

540 (18) Yoon, S.; Nissen, S.; Park, D.; Sanford, R. A.; Löffler, F. E. Nitrous Oxide Reduction
541 Kinetics Distinguish Bacteria Harboring Clade I NosZ from Those Harboring Clade II
542 NosZ. *Appl Environ Microbiol* **2016**, *82* (13), 3793–3800.
543 https://doi.org/10.1128/AEM.00409-16.

544 (19) Zhou, Y.; Suenaga, T.; Qi, C.; Riya, S.; Hosomi, M.; Terada, A. Temperature and Oxygen
545 Level Determine N_2O Respiration Activities of Heterotrophic N_2O-reducing Bacteria:
546 Biokinetic Study. *Biotechnol Bioeng* **2021**, *118* (3), 1330–1341.
547 https://doi.org/10.1002/bit.27654.

548 (20) Conthe, M.; Wittorf, L.; Kuenen, J. G.; Kleerebezem, R.; Hallin, S.; van Loosdrecht, M. C.
549 M. Growth Yield and Selection of *NosZ* Clade II Types in a Continuous Enrichment Culture
550 of N_2O Respiring Bacteria. *Environ Microbiol Rep* **2018**, *10* (3), 239–244.
551 https://doi.org/10.1111/1758-2229.12630.

552 (21) Hein, S.; Simon, J. Bacterial Nitrous Oxide Respiration: Electron Transport Chains and
553 Copper Transfer Reactions; 2019; pp 137–175.
554 https://doi.org/10.1016/bs.ampbs.2019.07.001.

555 (22) Hallin, S.; Philippot, L.; Löffler, F. E.; Sanford, R. A.; Jones, C. M. Genomics and Ecology
556 of Novel N_2O-Reducing Microorganisms. *Trends Microbiol* **2018**, *26* (1), 43–55.
557 https://doi.org/10.1016/j.tim.2017.07.003.

558 (23) Bertagnolli, A. D.; Konstantinidis, K. T.; Stewart, F. J. Non-denitrifier Nitrous Oxide
559 Reductases Dominate Marine Biomes. *Environ Microbiol Rep* **2020**, *12* (6), 681–692.
560 https://doi.org/10.1111/1758-2229.12879.

561 (24) Orellana, L. H.; Rodriguez-R, L. M.; Higgins, S.; Chee-Sanford, J. C.; Sanford, R. A.;
562 Ritalahti, K. M.; Löffler, F. E.; Konstantinidis, K. T. Detecting Nitrous Oxide Reductase
563 (*NosZ*) Genes in Soil Metagenomes: Method Development and Implications for the
564 Nitrogen Cycle. *mBio* **2014**, *5* (3). https://doi.org/10.1128/mBio.01193-14.

565 (25) Lui, L. M.; Majumder, E. L.-W.; Smith, H. J.; Carlson, H. K.; von Netzer, F.; Fields, M.
566 W.; Stahl, D. A.; Zhou, J.; Hazen, T. C.; Baliga, N. S.; Adams, P. D.; Arkin, A. P.
567 Mechanism Across Scales: A Holistic Modeling Framework Integrating Laboratory and
568 Field Studies for Microbial Ecology. *Front Microbiol* **2021**, *12*.
569 https://doi.org/10.3389/fmicb.2021.642422.

570 (26) Yu, L.; Harris, E.; Lewicka-Szczebak, D.; Barthel, M.; Blomberg, M. R. A.; Harris, S. J.;
571 Johnson, M. S.; Lehmann, M. F.; Liisberg, J.; Müller, C.; Ostrom, N. E.; Six, J.; Toyoda,
572 S.; Yoshida, N.; Mohn, J. What Can We Learn from N_2O Isotope Data? – Analytics,
573 Processes and Modelling. *Rapid Communications in Mass Spectrometry* **2020**, *34* (20).
574 https://doi.org/10.1002/rcm.8858.

575 (27) Lim, N. Y. N.; Frostegård, Å.; Bakken, L. R. Nitrite Kinetics during Anoxia: The Role of
576 Abiotic Reactions versus Microbial Reduction. *Soil Biol Biochem* **2018**, *119*, 203–209.
577 https://doi.org/10.1016/j.soilbio.2018.01.006.

578 (28) Green, S. J.; Prakash, O.; Jasrotia, P.; Overholt, W. A.; Cardenas, E.; Hubbard, D.; Tiedje,
579 J. M.; Watson, D. B.; Schadt, C. W.; Brooks, S. C.; Kostka, J. E. Denitrifying Bacteria from
580 the Genus Rhodanobacter Dominate Bacterial Communities in the Highly Contaminated
581 Subsurface of a Nuclear Legacy Waste Site. *Appl Environ Microbiol* **2012**, *78* (4), 1039–
582 1047. https://doi.org/10.1128/AEM.06435-11.

583 (29) Peng, M.; Wang, D.; Lui, L. M.; Nielsen, T.; Tian, R.; Kempher, M. L.; Tao, X.; Pan, C.;
584 Chakraborty, R.; Deutschbauer, A. M.; Thorgersen, M. P.; Adams, M. W. W.; Fields, M.
585 W.; Hazen, T. C.; Arkin, A. P.; Zhou, A.; Zhou, J. Genomic Features and Pervasive
586 Negative Selection in *Rhodanobacter* Strains Isolated from Nitrate and Heavy Metal
587 Contaminated Aquifer. *Microbiol Spectr* **2022**, *10* (1).
588 https://doi.org/10.1128/spectrum.02591-21.

589 (30) Van Den Heuvel, R. N.; Van Der Biezen, E.; Jetten, M. S. M.; Hefting, M. M.; Kartal, B.
590 Denitrification at PH 4 by a Soil-Derived Rhodanobacter-Dominated Community. *Environ*
591 *Microbiol* **2010**, *12* (12), 3264–3271. https://doi.org/10.1111/j.1462-2920.2010.02301.x.

592 (31) Smith, M. B.; Rocha, A. M.; Smillie, C. S.; Olesen, S. W.; Paradis, C.; Wu, L.; Campbell,
593 J. H.; Fortney, J. L.; Mehlhorn, T. L.; Lowe, K. A.; Earles, J. E.; Phillips, J.; Techtmann, S.

594 M.; Joyner, D. C.; Elias, D. A.; Bailey, K. L.; Hurt, R. A.; Preheim, S. P.; Sanders, M. C.;
595 Yang, J.; Mueller, M. A.; Brooks, S.; Watson, D. B.; Zhang, P.; He, Z.; Dubinsky, E. A.;
596 Adams, P. D.; Arkin, A. P.; Fields, M. W.; Zhou, J.; Alm, E. J.; Hazen, T. C. Natural
597 Bacterial Communities Serve as Quantitative Geochemical Biosensors. *mBio* **2015**, *6* (3).
598 https://doi.org/10.1128/mBio.00326-15.

599 (32) Moon, J.-W.; Paradis, C. J.; Joyner, D. C.; von Netzer, F.; Majumder, E. L.; Dixon, E. R.;
600 Podar, M.; Ge, X.; Walian, P. J.; Smith, H. J.; Wu, X.; Zane, G. M.; Walker, K. F.;
601 Thorgersen, M. P.; Poole II, F. L.; Lui, L. M.; Adams, B. G.; De León, K. B.; Brewer, S.
602 S.; Williams, D. E.; Lowe, K. A.; Rodriguez, M.; Mehlhorn, T. L.; Pfiffner, S. M.;
603 Chakraborty, R.; Arkin, A. P.; Wall, J. D.; Fields, M. W.; Adams, M. W. W.; Stahl, D. A.;
604 Elias, D. A.; Hazen, T. C. Characterization of Subsurface Media from Locations Up- and
605 down-Gradient of a Uranium-Contaminated Aquifer. *Chemosphere* **2020**, *255*, 126951.
606 https://doi.org/10.1016/j.chemosphere.2020.126951.

607 (33) Christiansen, J. R.; Outhwaite, J.; Smukler, S. M. Comparison of CO_2, CH_4 and N_2O Soil-
608 Atmosphere Exchange Measured in Static Chambers with Cavity Ring-down Spectroscopy
609 and Gas Chromatography. *Agric For Meteorol* **2015**, *211–212*, 48–57.
610 https://doi.org/10.1016/j.agrformet.2015.06.004.

611 (34) Sigman, D. M.; Casciotti, K. L.; Andreani, M.; Barford, C.; Galanter, M.; Böhlke, J. K. A
612 Bacterial Method for the Nitrogen Isotopic Analysis of Nitrate in Seawater and Freshwater.
613 *Anal Chem* **2001**, *73* (17), 4145–4153. https://doi.org/10.1021/ac010088e.

614 (35) Casciotti, K. L.; Sigman, D. M.; Hastings, M. G.; Böhlke, J. K.; Hilkert, A. Measurement
615 of the Oxygen Isotopic Composition of Nitrate in Seawater and Freshwater Using the
616 Denitrifier Method. *Anal Chem* **2002**, *74* (19), 4905–4912.
617 https://doi.org/10.1021/ac020113w.

618 (36) McIlvin, M. R.; Altabet, M. A. Chemical Conversion of Nitrate and Nitrite to Nitrous Oxide
619 for Nitrogen and Oxygen Isotopic Analysis in Freshwater and Seawater. *Anal Chem* **2005**,
620 *77* (17), 5589–5595. https://doi.org/10.1021/ac050528s.

621 (37) Lui, L. M.; Nielsen, T. N.; Smith, H. J.; Chandonia, J.-M.; Kuehl, J.; Song, F.; Sczesnak,
622 A.; Hendrickson, A.; Hazen, T.; Fields, M.; Arkin, A. P. Sediment and Groundwater
623 Metagenomes from Subsurface Microbial Communities from the Oak Ridge National
624 Laboratory Field Research Center, Oak Ridge, TN, USA. *Res Sq* **2024**.

625 (38) Wu, X.; Gushgari-Doyle, S.; Lui, L. M.; Hendrickson, A. J.; Liu, Y.; Jagadamma, S.;
626 Nielsen, T. N.; Justice, N. B.; Simmons, T.; Hess, N. J.; Joyner, D. C.; Hazen, T. C.; Arkin,
627 A. P.; Chakraborty, R. Distinct Depth-Discrete Profiles of Microbial Communities and
628 Geochemical Insights in the Subsurface Critical Zone. *Appl Environ Microbiol* **2023**, *89*
629 (6). https://doi.org/10.1128/aem.00500-23.

630 (39) Nurk, S.; Meleshko, D.; Korobeynikov, A.; Pevzner, P. A. MetaSPAdes: A New Versatile
631 Metagenomic Assembler. *Genome Res* **2017**, *27* (5), 824–834.
632 https://doi.org/10.1101/gr.213959.116.

633 (40) Prjibelski, A.; Antipov, D.; Meleshko, D.; Lapidus, A.; Korobeynikov, A. Using SPAdes De Novo Assembler. *Curr Protoc Bioinformatics* **2020**, *70* (1). https://doi.org/10.1002/cpbi.102.

636 (41) *BBtools: 2016. BBTools. DOE Joint Genome Institute. https://jgi.doe.gov/data-and-tools/software-tools/bbtools/. Retrieved 25 July 2023.*

638 (42) Hyatt, D.; Chen, G.-L.; LoCascio, P. F.; Land, M. L.; Larimer, F. W.; Hauser, L. J. Prodigal: Prokaryotic Gene Recognition and Translation Initiation Site Identification. *BMC Bioinformatics* **2010**, *11* (1), 119. https://doi.org/10.1186/1471-2105-11-119.

641 (43) Cantalapiedra, C. P.; Hernández-Plaza, A.; Letunic, I.; Bork, P.; Huerta-Cepas, J. EggNOG-Mapper v2: Functional Annotation, Orthology Assignments, and Domain Prediction at the Metagenomic Scale. *Mol Biol Evol* **2021**, *38* (12), 5825–5829. https://doi.org/10.1093/molbev/msab293.

645 (44) Li, H.; Durbin, R. Fast and Accurate Short Read Alignment with Burrows–Wheeler Transform. *Bioinformatics* **2009**, *25* (14), 1754–1760. https://doi.org/10.1093/bioinformatics/btp324.

648 (45) Stępniewski, W.; Sobczuk, H.; Widomski, M. Diffusion in Soils; 2011; pp 214–220. https://doi.org/10.1007/978-90-481-3585-1_273.

650 (46) Baldocchi, D.; Chu, H.; Reichstein, M. Inter-Annual Variability of Net and Gross Ecosystem Carbon Fluxes: A Review. *Agric For Meteorol* **2018**, *249*, 520–533. https://doi.org/10.1016/j.agrformet.2017.05.015.

653 (47) Hicks Pries, C. E.; Castanha, C.; Porras, R. C.; Torn, M. S. The Whole-Soil Carbon Flux in Response to Warming. *Science (1979)* **2017**, *355* (6332), 1420–1423. https://doi.org/10.1126/science.aal1319.

656 (48) Wu, Y.; Whitaker, J.; Toet, S.; Bradley, A.; Davies, C. A.; McNamara, N. P. Diurnal Variability in Soil Nitrous Oxide Emissions Is a Widespread Phenomenon. *Glob Chang Biol* **2021**, *27* (20), 4950–4966. https://doi.org/10.1111/gcb.15791.

659 (49) Wu, S.; Chen, J.; Li, C.; Kong, D.; Yu, K.; Liu, S.; Zou, J. Diel and Seasonal Nitrous Oxide Fluxes Determined by Floating Chamber and Gas Transfer Equation Methods in Agricultural Irrigation Watersheds in Southeast China. *Environ Monit Assess* **2018**, *190* (3), 122. https://doi.org/10.1007/s10661-018-6502-0.

663 (50) Wittorf, L.; Bonilla-Rosso, G.; Jones, C. M.; Bäckman, O.; Hulth, S.; Hallin, S. Habitat Partitioning of Marine Benthic Denitrifier Communities in Response to Oxygen Availability. *Environ Microbiol Rep* **2016**, *8* (4), 486–492. https://doi.org/10.1111/1758-2229.12393.

667 (51) Sanford, R. A.; Wagner, D. D.; Wu, Q.; Chee-Sanford, J. C.; Thomas, S. H.; Cruz-García, C.; Rodríguez, G.; Massol-Deyá, A.; Krishnani, K. K.; Ritalahti, K. M.; Nissen, S.; Konstantinidis, K. T.; Löffler, F. E. Unexpected Nondenitrifier Nitrous Oxide Reductase

670 Gene Diversity and Abundance in Soils. *Proceedings of the National Academy of Sciences*
671 **2012**, *109* (48), 19709–19714. https://doi.org/10.1073/pnas.1211238109.

672 (52) Hénault, C.; Bourennane, H.; Ayzac, A.; Ratié, C.; Saby, N. P. A.; Cohan, J.-P.; Eglin, T.;
673 Gall, C. Le. Management of Soil PH Promotes Nitrous Oxide Reduction and Thus Mitigates
674 Soil Emissions of This Greenhouse Gas. *Sci Rep* **2019**, *9* (1), 20182.
675 https://doi.org/10.1038/s41598-019-56694-3.

676

677